國立交通大學

電子物理學系

碩士論文

奈米元件的熱電性質

Thermoelectric properties

in molecular and atomic nanojunctions

研究生：陳譯仁

指導教授：陳煜璋　教授

中華民國 98 年 7 月

奈米元件的熱電性質

Thermoelectric properties

in molecular and atomic nanojunctions

研 究 生：陳譯仁　　Student：Yi-Ren Chen

指導教授：陳煜璋　　Advisor：Yu-Chang Chen

國 立 交 通 大 學

電 子 物 理 學 系

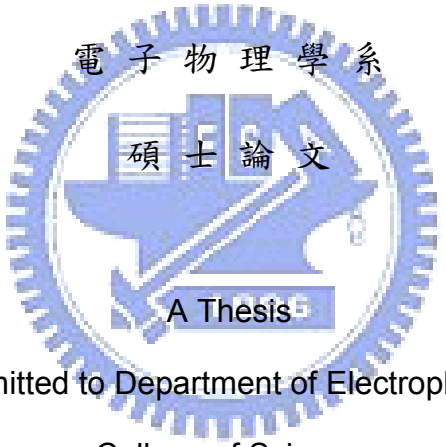

碩 士 論 文

A Thesis

Submitted to Department of Electrophysics

College of Science

National Chiao Tung University

in partial Fulfillment of the Requirements

for the Degree of Master

July 2009

Hsinchu, Taiwan, Republic of China

中華民國 98 年 7 月

奈米元件的熱電性質

研 究 生：陳譯仁　　指導教授：陳煜璋

國立交通大學電子物理學系

摘要

應用第一原理計算的方法，我們研究了分子熱電元件在趨近零外加偏壓和有外加偏壓情兩種不同況下的熱電性質。在利用 butanethiol 為實驗對象下，我們發現有用氨基取代的 butanethiol 和沒有取代的 butanethiol，它們的 Seebeck 係數會呈現非常大的不同。而且若把閘極電壓加下去我們還能調控 Seebeck 係數使它達到最佳化。在有用氨基取代的 butanethiol 下我們發現調控外加偏壓和閘極偏壓可以改變 Seebeck 係數的正負號，這意味著我們可以改變分子熱電元件的導電狀態，從 N 型到 P 型。除了 Seebeck 係數以外，整個熱電元件的轉換效率也是我們所關心的。熱電轉化效率重要的指標為 ZT，我們在趨近零外加偏壓和兩邊電極溫度差趨近於零的情況下對碳原子線和鋁原子線的系統做了一些研究。我們發現當電極溫度遠小於特徵溫度$T_0 = \sqrt{\frac{\beta}{\gamma(\ell)}}$時$ZT \propto T^2$；相對的，當電極溫度遠大於特徵溫度時 ZT 會趨於飽和。而且 ZT 和原子線長度是有相依性的並不會和長度(原子數目)無關。鋁原子線越長 ZT 就越大；相反的，碳原子線越長 ZT 就越小。這應該是和一個是導體一個是非導體有很大的關係。同時我們在研究 Seebeck 係數和

ZT 也注意到鋁原子線有很強的元件性質(跟元件形狀有關)而碳原子線則有部分的元件性質(Seebeck 係數和碳原子線長度無關)。這是個有趣的現象，我們希望能藉著更多的研究數據來找出其背後更多新的物理。

Thermoelectric properties

in molecular and atomic nanojunctions

Student: Yi-Ren Chen Advisor: Yu-Chang Chen

Department of Electrophysics
National Chiao Tung University

Abstract

A field-theoretic theory combined with first-principles approaches is presented for the thermoelectricity in molecular junctions formed by a single molecule contact. The study compares the Seebeck coefficient in the amino-substituted and unsubstituted butanethiol junction and observes interesting thermoelectric properties in the amino-substituted junction. Due to the novel states around the Fermi levels introduced by the amino-substitution, the Seebeck coefficient could easily be controlled using gate voltages and

biases. When the temperature in one of the electrodes is fixed, the Seebeck coefficient varies pronouncedly with the temperature in the other electrode, and such dependence could be enhanced by varying gate voltages. At large biases, richer features in the Seebeck coefficient are observed, which are closely related to the density of states in the vicinity of the left and right Fermi levels. In addition, we investigated the efficiency of energy conversion in nanojunctions, described by the thermoelectric figure of merit ZT. We obtained the qualitative and quantitative descriptions for the dependence of ZT on temperatures and lengths. A characteristic temperature: $T_0 = \sqrt{\frac{\beta}{\gamma(\ell)}}$ was observed. When $T \ll T_0$, $ZT \propto T^2$. When $T \gg T_0$, ZT tends to a saturation value. The dependence of ZT on the wire length for the metallic atomic chains is opposite to that for the insulating molecules: for aluminum atomic (conducting) wires, the saturation value of ZT increases as the length increases; while for alkanethiol (insulating) chains, the saturation value of ZT decreases as the length increases. We show that the thermoelectric quantities in nanojunctions unnecessarily display material properties. The Seebeck coefficient and the thermoelectric figure of merit are shows that metallic atomic chains reveal strong junction properties while the insulating molecular wires partially possess the material properties.

Acknowledgments

There are so many people that have helped me on the path to my master's degree. Firstly, I must offer my deep thanks to my advisor, Prof. Chen. He taught me the base of first-principle calculation in nanojunctions, and the method to study the novel field about the thermoelectric effects in nanoscale device, which is very different from mesoscopic and macroscopic scales. And he gave me a lot of suggestions when I met some difficulties on my research. Secondly I thank to Dr. Y. S. Liu, he is a experienced researcher and a kind people, gave me a lot of help. Thirdly I thank to my group partners, who gave me a lot of help in how to run program when I am a newcomer. Anyway I get knowledge from them and I thank them so much.

Contents

List of Figures

Chapter 1 Introduction

Nanoscale thermoelectric devices may be considered as new types of devices which may be embedded into integrated chip set to assist the stability of devices by converting the accumulated waste heat into useful electric energy. There has been ever increasing interest in the thermoelectric properties in nanojunctions. In addition, the experimental measurements of Seebeck coefficient in molecular nanojunction are presented recently, that is the principal motive for our theory calculation[1,2,3] of molecular nanojunction. Because the Seebeck coefficients are relevant not only to the magnitude but also to the slope of density of states (DOSs), the Seebeck coefficients can reveal more detailed information about the electronic structures of the materials in nanojunctions beyond the conductance measurements can provide. The Seebeck coefficients have been applied to explore the electronic structures of molecular junctions using functional substitutions for the bridging molecules. Theorists have proposed using the gate fields and external biases as a means to modulate the Seebeck coefficient in nanojunctions.

1-1 Thermoelectric effects

1-1-1 Thermoelectric figure of merit

In 1912, Altenkirch[4,5] introduced the concept of thermoelectric figure of merit when he showed that good thermoelectric materials should possess large Seebeck coefficients, high electrical conductivity to minimize Joule heating and low thermal conductivity to retain heat at the junctions that will help maintain a large temperature gradient. Ioffe in 1957[6] described the quality the efficiency of thermoelectric materials using the figure of merit as[7]

$$ZT = \frac{S^2\sigma}{\kappa_{el} + \kappa_{ph}} T , \quad (1)$$

where S is Seebeck coefficient[3,8], σ is the electrical conductivity, κ_{el} is electron thermal conductivity, κ_{ph} is phonon thermal conductivity and T is average temperature in the source-drain electrodes. The ideal thermoelectric material would have a large S, a large σ and a small κ_{ph} and κ_{el}. Increasing the electrical thermal conductivity usually leads to a simultaneous increase in the electrical heat conductivity. Therefore, how to enhance ZT for thermoelectric materials is a very challenging problem.

1-1-2 History of thermoelectric effects

There are three reversible thermoelectric effects in physics: Seebeck effect, Peltier effect and Thomson effect. The history of them was described respectively as below.

When two ends of a wire are held at different temperatures, a voltage develops across the two sides. This effect is known as the Seebeck effect , which was discovered by Seebeck in 1821 and published in 1822[9].

The Seebeck coefficient can be defined as the temperature gradient of the voltage:

$$S = \frac{\Delta V}{\Delta T} . \quad (2)$$

In 1834, the Peltier effect, a companion to the Seebeck effect, was discovered[10]. This effect occurs when a current passes through a wire. The current will carry thermal energy so that the temperature of one end of the wire decreases and the other increases. The Peltier coefficient $\prod_{12}$ is defined as the heat emitted per unit time per unit current flow from conductor 1 to 2. Therefore, this heat is directly proportional to the current passing through the junction as

below:

$$dQ = \prod dI , \tag{3}$$

where dQ is the heat current carried by current dI. The Peltier effect is often overwhelmed by irreversible Joule heating, which also originates from electronic current.

The Thomson effect was predicted in 1854 and found experimentally in 1856[11]. The Thomson effect occurs when a current flows across two points of a homogeneous wire having a temperature gradient along its length and heat is emitted or absorbed in addition to the Joule heat. The Thomson coefficient μ_T is positive if heat is generated when positive current flows from a higher temperature to lower temperature.

$$dQ = \mu_T \frac{\partial T}{\partial x} dx dI . \tag{4}$$

The three thermal-electrical properties provide the basis for modern direct energy conversion devices and their exploitation has been the subject of considerable research.

1-2 Experimental findings

Thermoelectric effects were observed long time ago. The macroscopic and microscopic models have been well developed and have been able to successfully explain the thermoelectric properties in the bulk materials. In the past few decades, thermoelectricity has gained renewal interests due to the progress in growing micro and nano structures, such as quantum well, super lattice, and quantum dot. Small structure can significantly alter the features of density of states by changing the dimensionality. Thus, it leads to novel thermoelectric properties beyond the bulk materials. The efficiency of energy

conversion could be enhanced due to the enhancement of the Seebeck coefficient by small structures in materials.

Although extensive researches have been made on electron transport in the nanoscale junctions, the thermoelectricity in molecular junctions has never been measured until very recent. In 2007, Prof. Majumdar's[12,13,14] group at UC, Berkeley has measured the Seebeck coefficients in a single-molecule junction and demonstrated the capability to fabricate the thermoelectric molecular devices. These experiments open a new era to study the thermoelectric effects at atomic level.

Majumdar's experimental setup is shown schematically in Fig.1 [12].

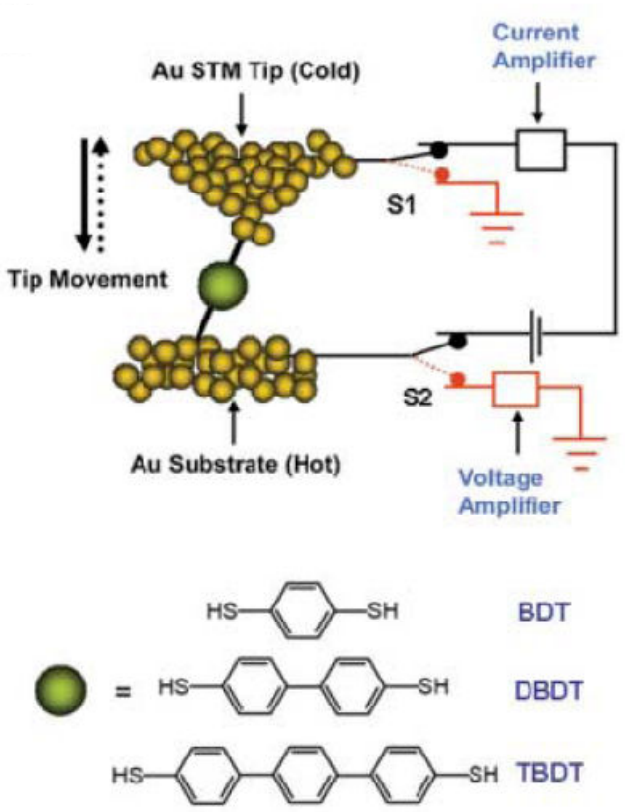

Fig. 1. Schematic description of the experimental set up based on an STM break junction. Molecules of BDT, DBDT, or TBDT are trapped between the Au STM tip kept at ambient temperature and a heated Au substrate kept at temperature ΔT above the ambient. When the tip approaches the substrate, a voltage bias is applied and the current is monitored to estimate the conductance. When the conductance reaches a threshold of 0.1 G_0, the voltage bias and the current amplifier are disconnected. A voltage amplifier is then used to measure the induced thermoelectric voltage, ΔV, and the tip is gradually pulled away from the substrate. **[12]**

The result they get was: Seebeck coefficients is independent of the number of molecules is shown in Fig.2 [12], the length dependence of molecular junction Seebeck coefficients is shown in Fig.3 [12], and Seebeck coefficients reveal more detailed information about the electronic structures of the molecule sandwiched in the nanojunctions beyond what the conductance measurements can provide is shown in Fig.4 [12].

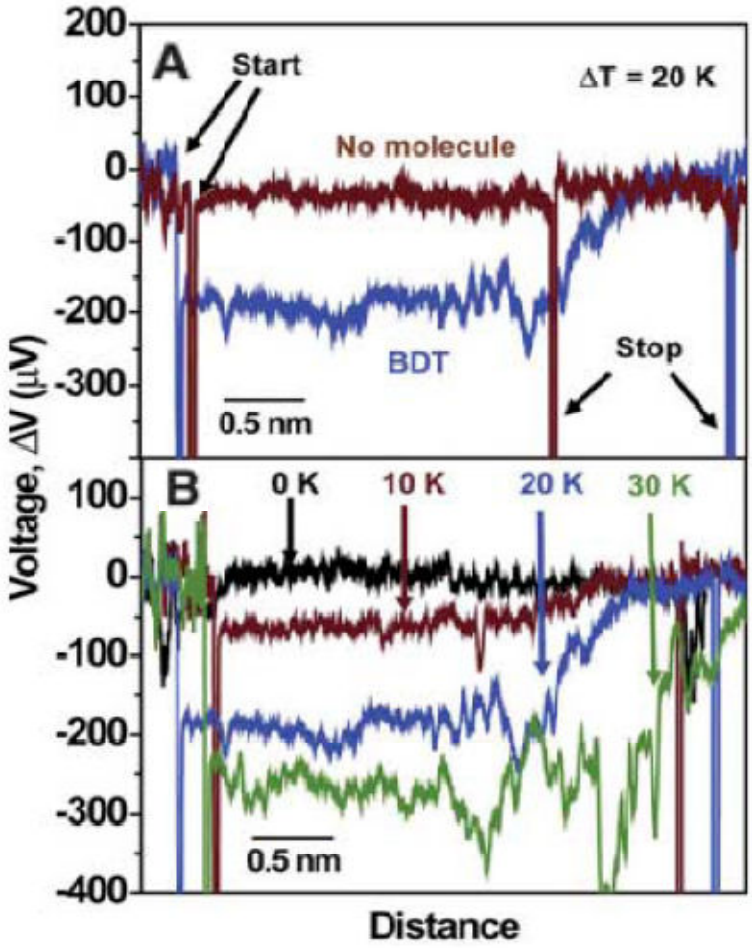

Fig. 2. (A) A plot of the thermoelectric voltage measured as a function of the tip-sample distance when a temperature differential ΔT= 20 K is applied (Au tip at ambient and substrate at ambient + 20 K). The blue curve is obtained when a Au-BDT-Au junction is broken. The red curve shows a control experiment performed on a clean gold substrate. **(B)** Typical thermoelectric voltage traces for tip-substrate temperature differentials of 0, 10, 20, and 30 K for Au-BDT-Au junctions. **[12]**

In Fig.2 [12], blue curve, they observed a constant thermoelectric voltage of about ΔV= -200 μV, which lasted until all of the molecules trapped in the junction broken away, suggesting that the Seebeck coefficient is independent of the number of molecules.

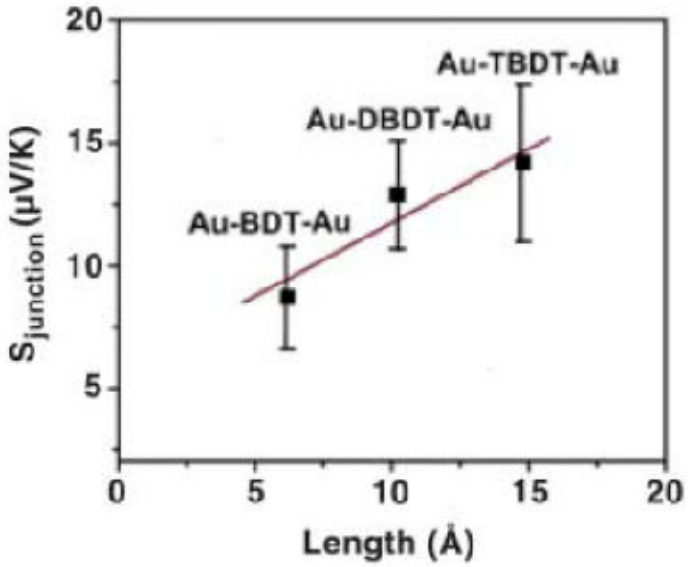

Fig. 3. Plot of measured junction Seebeck coefficient as a function of molecular length for BDT, DBDT, and TBDT. **[12]**

In Fig.3 [12], the experiment seems to show a linear dependence of the Seebeck coefficient on the molecular length. The Seebeck coefficients increase as the lengths of the molecules increase.

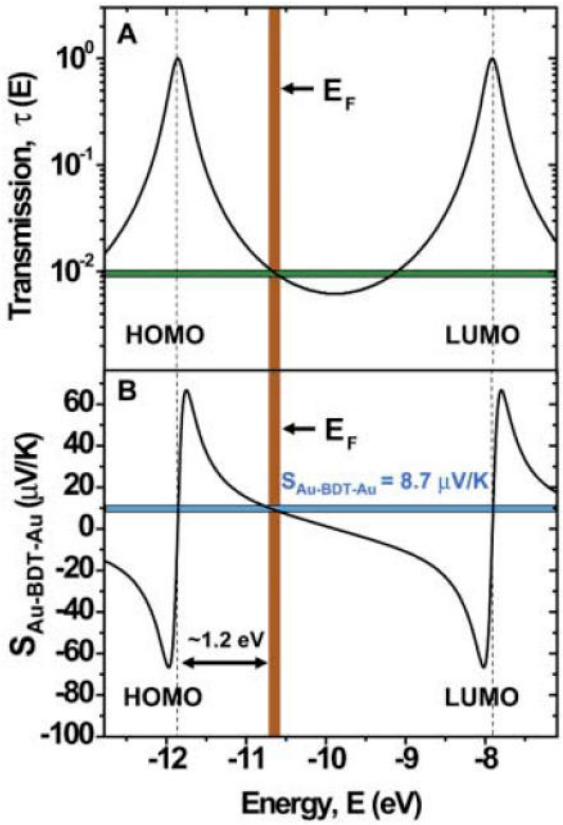

Fig. 4. Relating the measured Seebeck coefficient of Au-BDT-Au junction to the position of Fermi level. **(A)** theoretical prediction of the transmission function of a Au-BDT-Au junction plotted as a function of the relative position of the Fermi level of the Au electrodes with respect to the HOMO and LUMO levels. **(B)** The predicted Seebeck coefficient of a Au-BDT-Au junction as a function of the relative position of the Fermi level with respect to the HOMO and LUMO levels. When the measured value of $S_{Au\text{-}BDT\text{-}Au}$ = +8.7±2.1 μV/K (blue band) is shown, it is clear that the Fermi level is ~1.2 eV above the HOMO level. At this energy level, the transmission function is $\tau(E)\sim 0.01$. **[12]**

Measurements of the Seebeck coefficient in nanojunctions can provide insight into the electronic structure of the heterojunction. In Fig.4 [12], the Seebeck coefficient can be related to the transmission probability[15] according to the following relation:

$$S = -\frac{\pi^2 K_B^2 T}{3e}\frac{\partial \ln \tau(E)}{\partial E}\Big|_{E=E_F} \qquad (5)$$

As shown in Fig.4 [12], the positive value of the Seebeck coefficient may imply that the Fermi level of BDT is closer to HOMO.

Chapter 2 Theory

When the miniaturization of thermoelectric junctions reaches the atomic scale, it indeed opens new field for the thermoelectricity due to the quantum transport for electrons and phonons in atomistic system. Thus, the studies of thermoelectricity in molecular junctions require the development of new theories. Motivated by Majumdar's experiments, we develop theories allied to first-principles calculations to investigate the Seebeck coefficients and the thermoelectric figure of merit in the molecular tunneling junction.

2-1 Current of atomic wires[16]

We started by a brief introduction of the DFT calculations for a molecule sandwiched between two bulk electrodes with external source-drain bias. The effective single-particle wave functions of the whole system in the continuum states were calculated in scattering approach by solving the Lippmann-Schwinger equation with exchange and correlation energy included within the local density approximation. Two planar metallic electrodes, represented as a uniform-background (jellium) model.

The calculations proceeded in the following way: First, within the framework of the density-functional formalism, the single-particle wave functions and self-consistent density distribution were obtained by solving the coupled Poisson equation and Shrödinger equation for the pair of bare metallic electrodes in the presence of the bias voltage. Next, corresponding to each of these wave functions, a Lippmann-Schwinger equation involving a Green's function for the biased bimetallic junction was solved to obtain an effective single-particle wave function for the total system, consisting of the two electrodes plus a group of atoms. From these wave functions, the charge density for the total system was obtained, and the problem was solved self-consistently using a modified iterative procedure. Atomic units were used here, with $|e|=m=\hbar=1$.

2-1-1 Bimetal junction

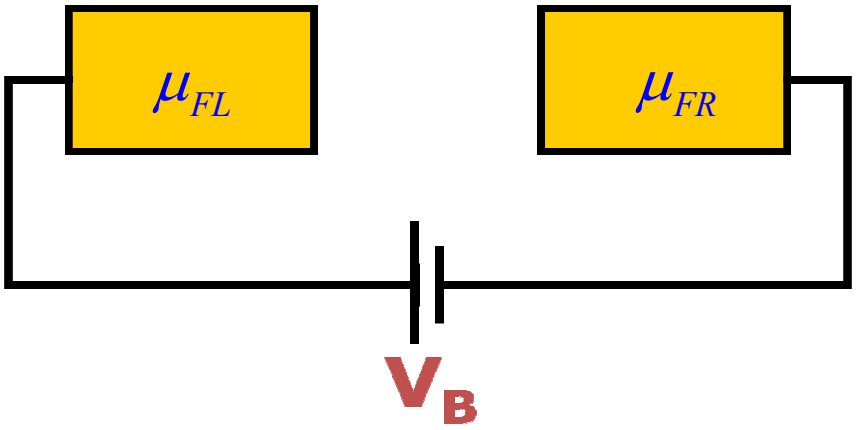

Fig. 5. The schematic of bimetal junction with external source-drain bias.

Two bulk electrodes are modeled as two semi-infinite bulk metals described by Jellium model. The wavefunction of the bare electrodes can be obtained by solving the Shrödinger equation and Poisson equation. Electrons incident from the left hand side can be partial transmitted and partially reflected. The unperturbed wavefunctions $\Psi^{M}_{EK_{\parallel}-}(r)$ of the electrons satisfy the boundary condition as shown in Eq. (7), i.e.,

$$\Psi^{M}_{EK_{\parallel}-}(\mathbf{r}) = e^{iK_{\parallel}\cdot R} u_{EK_{\parallel}-}(z), \tag{6}$$

where

$$u_{EK_{\parallel}-}(z) = \frac{1}{(2\pi)^{\frac{3}{2}}} k_R^{-\frac{1}{2}} \times \begin{cases} e^{-ik_R z} + Re^{ik_R z}, & z \to \infty \\ Te^{-ik_L z}, & z \to -\infty \end{cases}, \tag{7}$$

We first note that $\Psi^{M}(\mathbf{r})$, the superscripts M refer to the pair of bare biased metal electrodes, has the form $e^{iK_{\parallel}\cdot R} u_{EK_{\parallel}}(z)$, where R is the coordinate parallel to the surfaces and z the coordinate normal to them. Deep in the positively biased electrode (which we will take henceforth to be the left electrode), $u_{EK_{\parallel}}(z)$ has the form of a linear combination of left-moving and right-moving plane waves with wave vector k_L. Here, the energies of electrons are conservative as described by $\frac{1}{2}{k_L}^2 = E - \frac{1}{2}\left|\mathbf{K}_{\parallel}\right|^2 - u^{M}_{eff}(-\infty)$, where E is the energy eigenvalue

in the single-particle equations for the pair of biased electrodes and $u_{eff}^{M}(z)$ is the total effective potential (electrostatic plus exchange correlation).

Next we will specify the character of $u_{EK_{\parallel}}(z)$ by an additional subscript α: $u_{EK_{\parallel}\alpha}(z)$. For propagating states, we will replace α either by "+," which will correspond to a wave incident from the left (together with its reflected and transmitted parts) or by "−," which will correspond to a wave incident from the right and thus k_R is defined as $\frac{1}{2}{k_R}^2 = E - \frac{1}{2}\left|\mathbf{K}_{\parallel}\right|^2 - u_{eff}^{M}(\infty)$. The coefficient has been chosen to accord with the continuum normalization which we impose on the wave functions Ψ^{M}, specified by

$$\int d^3\mathbf{r}\left[\Psi^{M}_{E'\mathbf{K}'_{\parallel}\alpha}(\mathbf{r})\right]^{*}\Psi^{M}_{E\mathbf{K}_{\parallel}\alpha}(\mathbf{r}) = \delta(E-E')\delta(\mathbf{K}_{\parallel}-\mathbf{K}'_{\parallel})\,. \tag{8}$$

2-1-2 Metal-molecule-metal junction

We investigate the electron transport, phonon transport, and thermoelectricity of molecules wire and atomic wires[1] sandwiched between two bulk electrodes with finite external source-drain bias and finite temperature difference as shown in Fig. 6, where the bias is given by $V_B = \frac{\mu_{FR}-\mu_{FL}}{e}$.

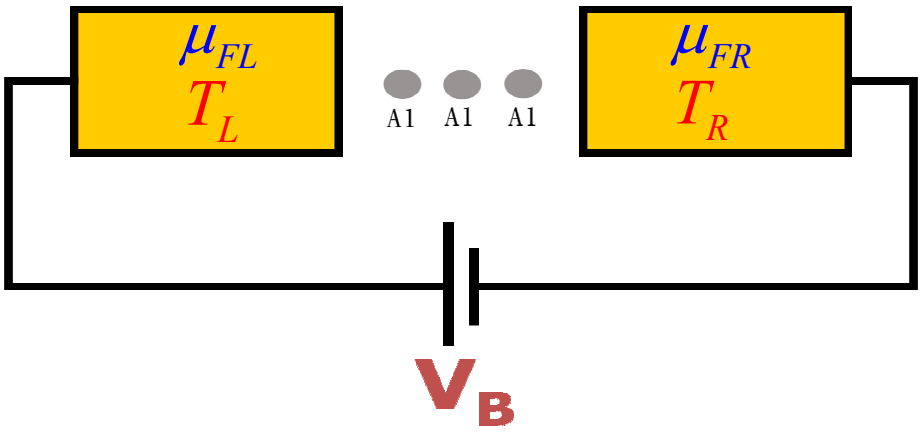

Fig. 6. The schematic of aluminum atomic junction: the atomic size conductors where both chemical potential and temperature gradients are present.

The continuum wave functions Ψ^{MA}, the superscripts MA refer to the complete system consisting of the metal electrodes and the group of atoms between them, are solved in scattering approaches. The continuum wave functions Ψ^{MA} are solved by the Lippmann-Schwinger equation, where Ψ^{M} will have the same labeling $(E, \mathbf{K}_{\parallel}, \alpha)$, even though $\mathbf{K}_{\parallel}$ no longer refers to a conserved quantity. These solutions will also have the same normalization as the Ψ^{M}, a fact that facilitates the calculation of the electron density distribution and the current. For $E_{FL} < E < E_{FR}$, where E_{FL} is the Fermi level in the left electrode and $E_{FR} = E_{FL} + V_B$ is the Fermi level in the right electrode (bias V_B taken positive), we occupy only states corresponding to a wave incident from the right, i.e., only $\Psi^{MA}_{E\mathbf{K}_{\parallel}-}$ and not $\Psi^{MA}_{E\mathbf{K}_{\parallel}+}$.

The Hamilton of complete system can be put into Lippmann-Schwinger form :

$$\Psi^{MA}(\mathbf{r}) = \Psi^{M}(\mathbf{r}) + \int d^3\mathbf{r}'\, d^3\mathbf{r}''\, G^{M}(\mathbf{r}, \mathbf{r}')\delta V(\mathbf{r}', \mathbf{r}'')\Psi^{MA}(\mathbf{r}''), \qquad (9)$$

this equation embodies the motion that electrons in states of the electrodes impinge on and are scattered elastically by the potential $\delta V(\mathbf{r}, \mathbf{r}')$, which describes the difference in potential between the complete system and the bare electrodes. It can be written

$$\delta V(\mathbf{r}, \mathbf{r}') = v_{ps}(\mathbf{r}, \mathbf{r}') + \left[v_{xc}\left(n^{MA}(\mathbf{r})\right) - v_{xc}\left(n^{M}(\mathbf{r})\right) + \int d^3\mathbf{r}'' \frac{\delta n(\mathbf{r}'')}{|\mathbf{r} - \mathbf{r}''|}\right]\delta(\mathbf{r} - \mathbf{r}'), \qquad (10)$$

the term $v_{ps}(\mathbf{r}, \mathbf{r}')$ is the sum of the (nonlocal) pseudopotentials representing the atomic cores, $v_{xc}(n(\mathbf{r}))$ is the exchange-correlation potential, $n^{M}(\mathbf{r})$ is the electron number density for the pair of biased metal electrodes, $n^{MA}(\mathbf{r})$ is the density for the complete system, and $\delta n(\mathbf{r}) = n^{MA}(\mathbf{r}) - n^{M}(\mathbf{r})$. We will use the atomic pseudopotentials introduced by Hamann[17].

2-1-3 Current in nanojunction

First, we calculate the current with left/right electrode temperature at 0K, Fermi-Dirac distribution equal to 1. The electron number density is given by the sum of squares of the occupied states $\Psi^{MA}_{EK_{\parallel}\alpha}$, with a factor 2 included for spin degeneracy (we take the system to be unpolarized) the electric current density in the full system is given by

$$j^{MA}(\mathbf{r}) = -2\int_{E_{FL}}^{E_{FR}} dE \int d^2\mathbf{K}_{\parallel}\, \mathrm{Im}\left\{\left[\Psi^{MA}_{EK_{\parallel}-}(\mathbf{r})\right]^{*}\nabla\Psi^{MA}_{EK_{\parallel}-}(\mathbf{r})\right\}, \tag{11}$$

where the integral over $\mathbf{K}_{\parallel}$ is restricted by $|\mathbf{K}_{\parallel}| \le \sqrt{2[E - u^{M}_{eff}(\infty)]}$. Now let j^{M} be the current density for the pair of biased electrodes in the absence of the group of atoms. Then the quantity of interest to us is

$$I = \int d^2R\, \hat{z}\cdot[j^{MA} - j^{M}], \tag{12}$$

which is independent of z since our system has no current sources or sinks. Here $\hat{z}$ is the unit vector point to the right and perpendicular to the surfaces of the electrodes. If we write $\Psi^{MA} = \Psi^{M} + \delta\Psi$, then

$$I = -2\int_{E_{FL}}^{E_{FR}} dE \int d^2\mathbf{K}_{\parallel} \int d^2\,\mathbf{R}\, \mathrm{Im}\left\{\left[\Psi^{M}_{EK_{\parallel}-}(\mathbf{r})\right]^{*}\frac{d}{dz}\delta\Psi_{EK_{\parallel}-}(\mathbf{r}) + \delta\Psi^{*}_{EK_{\parallel}-}(\mathbf{r})\frac{d}{dz}\Psi^{M}_{EK_{\parallel}-}(\mathbf{r})\right.$$
$$\left. + \delta\Psi^{*}_{EK_{\parallel}-}(\mathbf{r})\frac{d}{dz}\delta\Psi_{EK_{\parallel}-}(\mathbf{r})\right\}, \tag{13}$$

where the integration range for $\mathbf{K}_{\parallel}$ is the same as in Eq. (11).

Next, we calculate the current trough the tunnel junction where the temperatures and chemical potentials in source and drain electrodes can be

different, Fermi-Dirac distribution not equal to 1 or 0.

$$I = -i\int dE \int d^2\mathbf{R} \int d^2\mathbf{K}_{\parallel} \left(f_E^L I_{EE}^{LL} + f_E^R I_{EE}^{RR} \right), \tag{14}$$

where

$$I_{EE'}^{ij} = \left[\Psi_E^i(\mathbf{r}, \mathbf{K}_{\parallel})\right]^* \nabla \Psi_{E'}^j(\mathbf{r}, \mathbf{K}_{\parallel}) - \nabla\left[\Psi_E^i(\mathbf{r}, \mathbf{K}_{\parallel})\right]^* \Psi_{E'}^j(\mathbf{r}, \mathbf{K}_{\parallel}), \tag{15}$$

where $i, j = L, R.$ $\Psi_E^{L(R)}(\mathbf{r}, \mathbf{K}_{\parallel})$ is the single-particle wave function incident from the left (right) electrode with energy E and component of the momentum $\mathbf{K}_{\parallel}$ parallel to the electrode surface[18,19], and $d^2\mathbf{R}$ represents an element of the electrode surface. We assume that the left/right electrode serves as the electron and thermal reservoir with the electron population described by the Fermi-Dirac distribution function

$$f_E^{L(R)}\left(\mu_{L(R)}, T_{L(R)}\right) = \frac{1}{\left(e^{\frac{E-\mu_{L(R)}}{k_B T_{L(R)}}} + 1\right)}, \tag{16}$$

where $\mu_{L(R)}$ and $T_{L(R)}$ are the chemical potential and the temperature in the left (right) electrode, respectively, and k_B is the Boltzmann constant. For simplicity, we define the transmission probability of electron with energy E incident from the left (right) electrode as

$$\tau^{L(R)}(E) = -i\pi \int d^2\mathbf{R} \int d^2\mathbf{K}_{\parallel}\, I_{EE}^{LL(RR)}(\mathbf{r}, \mathbf{K}_{\parallel}). \tag{17}$$

By using the relation $\tau(E) = \tau^R(E) = \tau^L(E)$, a direct consequence of the time-reversal symmetry, the current in Eq. (14) can be rewritten as

$$I(\mu_L, T_L, \mu_R, T_R) = \frac{1}{\pi}\int dE \left[f_E^R(\mu_R, T_R) - f_E^L(\mu_L, T_L)\right]\tau^R(E), \tag{18}$$

where the left and right electrode have different chemical potentials given by the bias (the source drain bias is $V_{SD} = \frac{\mu_R - \mu_L}{e}$) . We also assume that the left/right electrode can be connected to its own heat bath such that T_L can be different from T_R.

2-2 Thermoelectric figure of merit

Molecular tunneling junctions consist of source-drain electrodes as independent electron and heat reservoirs with distinct temperatures $T_{L(R)}$ and chemical potentials $\mu_{L(R)}$. The efficiency of energy conversion depends on several factors: the electrical conductance (σ), the Seebeck coefficient (S), the electron thermal conductance (κ_{el}) and the phonon thermal conductance (κ_{ph}). The efficiency can be described by the dimensionless thermoelectric figure of merit:

$$ZT = \frac{S^2\sigma}{\kappa_{el} + \kappa_{ph}} T, \tag{19}$$

where $T = (T_L + T_R)/2$ is the average temperature in the source-drain electrodes. The ideal thermoelectric molecular junction would have a large S, a large σ and a small combined thermal conductance ($\kappa_{el} + \kappa_{ph}$). Thermoelectric materials with a large σ are usually accompanied by a large κ_{el}, which makes the enhancement of the thermoelectric figure of merit a challenging task.

We reported theoretical calculations of the thermoelectric figure of merit in nanojunctions. It aimed to obtain a qualitative and quantitative descriptions of ZT for temperatures and lengths of the nanojunctions. The self-consistent density functional theory (DFT) was performed together with the derivation of an analytical expression for ZT to investigate its dependence on the temperatures and lengths of nanojunctions. The thermal current carried by electron transport and phonon transport were considered.

In the following subsections, we briefly introduce the Seebeck coefficient, the electrical conductance, the electron thermal conductance, and the phonon thermal conductance, respectively.

2-2-1 Seebeck coefficient[7,8]

Consider a tunnel junction (as mention above) that may have different temperatures in the source and drain electrodes, a small thermoelectric voltage (ΔV) in the junctions can be induced by an additional temperature difference (ΔT) applied in the electrodes. The ratio of the thermoelectric voltage to the temperature difference is defined as the Seebeck coefficient.

$$S = \frac{\Delta V}{\Delta T}. \tag{20}$$

From Eq. (18) and (20) when the system comes to equilibrium, the electric current generated by an additional infinitesimal temperature ΔT across the electrodes is compensated by an induced small voltage ΔV across the junction. For simplicity, we assume that the additional temperature and the induced voltage are distributed symmetrically in the left/right electrodes, that is,

$$I\left(\mu_L, T_L + \frac{\Delta T}{2}, \mu_R, T_R - \frac{\Delta T}{2}\right) + I\left(\mu_L + \frac{e\Delta V}{2}, T_L, \mu_R - \frac{e\Delta V}{2}, T_R\right)$$
$$= 2I(\mu_L, T_L, \mu_R, T_R), \tag{21}$$

where the electric current is given by Eq. (17) and (18). We can expand the Fermi-Dirac distribution function to the first order of ΔT and ΔV

$$f(E, \mu + e\Delta V, T + \Delta T) = f(E, \mu, T) + \frac{\partial}{\partial \mu} f(E, \mu, T) e\Delta V + \frac{\partial}{\partial T} f(E, \mu, T)\Delta T, \tag{22}$$

and then obtain the Seebeck coefficient in the linear response regime.

$$S(\mu_L, \mu_R, T_L, T_R) = -\frac{1}{e}\frac{\frac{K_1^L}{T_L} + \frac{K_1^R}{T_R}}{K_0^L + K_0^R}, \tag{23}$$

where

$$K_n^{L(R)} = -\int dE \left(E - \mu_{L(R)}\right)^n \frac{\partial f_E^{L(R)}}{\partial E} \tau(E)\,. \tag{24}$$

We can rewrite the above equation in a specific form

$$S(\mu_L, \mu_R, T_L, T_R) = -\frac{1}{e}\frac{\int \left(\frac{(E-\mu_L)}{T_L}\frac{\partial f_E^L(\mu_L, T_L)}{\partial E} + \frac{(E-\mu_R)}{T_R}\frac{\partial f_E^R(\mu_R, T_R)}{\partial E}\right)\tau(E)dE}{\int \left(\frac{\partial f_E^L(\mu_L, T_L)}{\partial E} + \frac{\partial f_E^R(\mu_R, T_R)}{\partial E}\right)\tau(E)dE}\,. \tag{25}$$

In the low temperature regime, where we neglect the higher order terms in the temperature, the above equation can be simplified using Sommerfeld expansion[8,12,20],

$$S(\mu_L, \mu_R, T_L, T_R) = -\frac{\pi^2 k_B^2 T_L \frac{\partial \tau(E)}{\partial E}\Big|_{E=\mu_L} + T_R \frac{\partial \tau(E)}{\partial E}\Big|_{E=\mu_R}}{3e\,\tau(\mu_L) + \tau(\mu_R)}\,, \tag{26}$$

which implies that the Seebeck coefficient is closely related to the slope of the transmission probability at Fermi level. When S>0, the carriers are p type. In this case the direction of electric current is the same as the direction of thermal current. When S<0, the carriers are n type. In this case, the direction of electric current is opposite to the direction of thermal current.

2-2-2 Electrical conductance

The electrical conductance, typically insensitive to temperature in cases that the direct tunneling is the major transport mechanism, may be expressed as

$\sigma = \frac{dI}{dV}$. Using Eq. (18), add e and $\hbar$ because we use atomic units before, and Eq. (22) we can get

$$I = \frac{2e^2}{h} K_0^{L(R)} \Delta V + \frac{2e}{h} K_1^{L(R)} \frac{\Delta T}{T}, \tag{27}$$

where $K_n^{L(R)} = -\int dE \left(E - \mu_{L(R)}\right)^n \frac{\partial f_E^{L(R)}}{\partial E} \tau(E)$.

In fact, here K_0 is the temperature dependent transmission function of the system. So the conductance with finite temperature is given as

$$\sigma = \frac{e}{2} \int \sum_{i=L,R} \frac{f_E^i \left(1 - f_E^i\right)}{K_B T_i} \tau(E) dE. \tag{28}$$

2-2-3 Electron thermal conductance

The thermal current conveyed by the transport electrons $J_{el}^{L(R)}$, via the following expressions:

$$J_{el}^{L(R)} = \frac{2}{h} \int dE \left[\left(E - \mu_{L(R)}\right)\left(f_E^R - f_E^L\right)\tau(E)\right]. \tag{29}$$

The electron thermal conductance (defined by $\kappa_{el} = \frac{\Delta J_{el}^{L(R)}}{\Delta T}$) can be calculate by Eq. (29) and (22), in the linear response regime and $T_L \approx T_R$ approximation.

$$\kappa_{el} = \frac{2}{h}\left(K_1 eS + \frac{K_2}{T}\right), \tag{30}$$

where $K_n = -\int dE (E - \mu)^n \frac{\partial f_E}{\partial E} \tau(E)$.

2-2-4 Phonon thermal conductance

So far, the physical quantities that have been discussed have been related to the propagation of electrons. However, in most cases, the thermal current is dominated by the contributions from phonon transport. In the absence of the phonon thermal conductance, the research on ZT is incomplete. To consider the phonon contribution to ZT, it is assumed that the nanojunction is a weak elastic link, with a given stiffness that may be evaluated from total energy calculations, attached to the electrodes modeled as phonon reservoirs. We estimate the contribution of the thermal current from phonon scattering (J_{ph}), following the approach of Patthon and Geller[21].

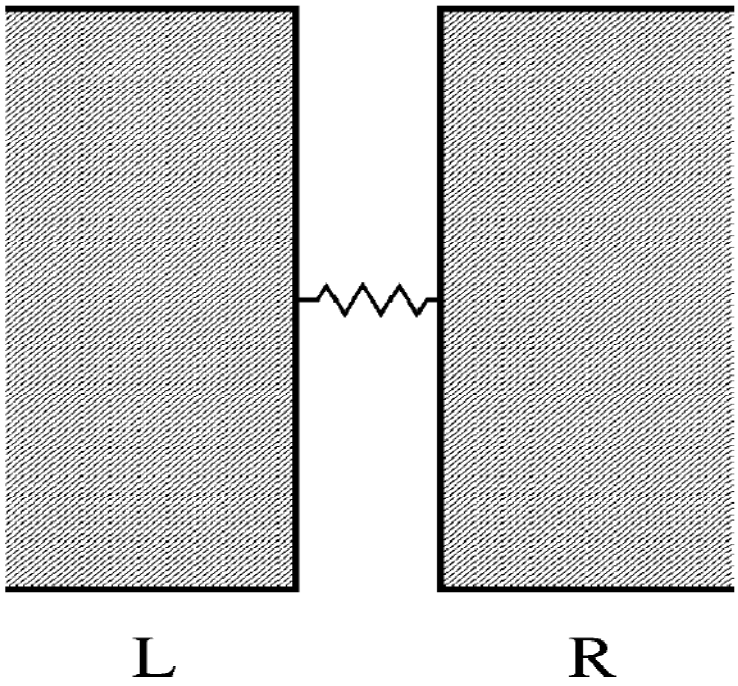

Fig. 7. Weak link model. Two macroscopic dielectrics, at temperatures T_L and T_R, are joined by a harmonic spring of stiffness K. **[21]**

The model we consider is shown in Fig.7 [21]: Two macroscopic solids L and R are held at fixed temperature T_L and T_R, each in thermodynamic equilibrium, and joined by a weak mechanically elastic link: a harmonic spring of stiffness K. The two bodies are assumed to be electrically insulating, so that thermal energy is carried only by phonons. In Patthon and Geller's paper we can get the formulation of the thermal current from phonon scattering (J_{ph}).

$$J_{ph} = \frac{2\pi K^2}{\hbar}\int_0^{\infty} dE\, E\, N_L(E) N_R(E)[n_L(E) - n_R(E)]\,, \qquad (31)$$

where $n_{L(R)} \equiv \frac{1}{e^{\frac{E}{K_B T_{L(R)}}-1}}$ and $N_{L(R)}(E) \simeq CE$ is the Bose-Einstein distribution function and the spectral density of phonon states in the left (right) electrode, respectively. After expanding the Bose-Einstein distribution function to the first order of ΔT in the expression of phonon thermal current, the phonon thermal conductance (defined by $\kappa_{ph} = \frac{\Delta J_{ph}}{\Delta T}$) is obtained

$$\kappa_{ph} = \frac{\pi K^2}{\hbar K_B}\int dE E^2 N_L(E)\, N_R(E) \sum_{i=L,R} \frac{n_i(E)\big(1 + n_i(E)\big)}{T_i^2}\,, \qquad (32)$$

where the stiffness of the bridging nano-structure is: $K = \frac{YA}{\ell}$, where Y is the Young's modulus and A (ℓ) is its cross-section (length). In the linear response regime and the $T_L \approx T_R$ approximation we can rewrite Eq. (32) as

$$\kappa_{ph} = \gamma(\ell) T^3\,, \quad \text{where } \gamma(\ell) = \frac{8\pi^5 K_B^4 C^2 A^2 Y^2}{15\hbar\ell^2}\,. \qquad (33)$$

2-2-5 ZT at linear response regime

In this subsection we aimed to obtain a qualitative and quantitative descriptions of ZT for temperatures and lengths of the nanojunctions in small bias and low temperature regimes. The results of this study may be of interest to experimentalists attempting to develop thermoelectric nanoscale devices.

The Seebeck coefficient and the electron (phonon) thermal conductance can be characterized by the power low expansions: $S \approx \alpha T$, $\kappa_{el} \simeq \beta\left[T + \eta T^3\right] \approx \beta T$ and $\kappa_{ph} = \gamma(\ell) T^3$ in the common range of temperatures($T_L \approx T_R = T$) and in

the linear response regime ($\mu_L \approx \mu_R = \mu$), where $\alpha = -\frac{\pi^2 K_B^2 \frac{\partial \tau(\mu)}{\partial E}}{3e\tau(\mu)}$; $\beta = \frac{2\pi^2 K_B^2 \tau(\mu)}{3h}$; $\eta = \frac{\left(\pi K_B \frac{\partial \tau(\mu)}{\partial E}\right)^2}{3\tau(\mu)^2}$ and $\gamma(\ell) = \frac{8\pi^5 K_B^4 C^2 A^2 Y^2}{15\hbar\ell^2}$. Consequently, ZT in the nanojunctions have a simple form

$$ZT \approx \frac{\alpha^2 \sigma T^3}{\beta T + \gamma(\ell) T^3}, \tag{34}$$

which is valid in small bias and low temperature regimes.

Chapter 3 Result and Discussion

3-1 Seebeck coefficient of Alkanethiol junctions[3]

3-1-1 Amino-substituted and unsubstituted butanethiol junctions

Alkanethiol $[CH_3(CH_2)_{n-1}SH$, denoted as $C_n]$-related molecules are a good representation of reproducible junctions that can be fabricated[22,23]. It has been established that nonresonant tunneling is the main conduction mechanism as Fermi levels of the two electrodes lie within the large HOMO-LUMO gap. However, functional group substitution may have significant effects on the electronic structures of alkanethiols. New states around the Fermi levels are produced when $–NH_2$ is substituted for –H in bridging butanethiol (C_4). The Seebeck coefficient as a function of the gate voltage for various temperatures in the amino-substituted and unsubstituted butanethiol junctions is presented in Fig. 8(a) [3]. The results show that the characteristics of the Seebeck coefficient are sensitive to the gate voltages in the amino-substituted butanethiol junction. The most striking feature is that the molecular transistor can be converted from n type to p type by applying the gate voltages. The Seebeck coefficient is close to zero at $V_G \approx -2.6\,V$. As the gate voltage further decreases, the sign of the Seebeck coefficient becomes positive (p type). For the butanethiol molecular junction, the characteristic of the carrier remains n type all the time because the sign of the Seebeck coefficient is negative.

To arrive at the physical reason why the gate voltage can efficiently modulate the Seebeck coefficient, the densities of states (DOSs) (transmission functions) are plotted as a function of energy for the various gate voltages in Fig.8(b) [3] (inset of Fig.8(b) [3]). We observe that the positive (negative) gate voltage shifts the LUMO peak toward higher (lower) energies. At $V_G = -2.6\,V$, the peak position of the LUMO and transmission function align with the Fermi levels implying that $\frac{\partial \ln \tau(E)}{\partial E}\Big|_{E=E_F} \approx 0$. Hence, the Seebeck coefficient is close to zero at

the gate voltage around $V_G = -2.6\,V$. When the gate voltage is tuned at around $V_G = 1.72\,V$, the Seebeck coefficient is negative because $\frac{\partial \ln\tau(E)}{\partial E}\Big|_{E=E_F} > 0$. Conversely, the Seebeck coefficient is positive because $\frac{\partial \ln\tau(E)}{\partial E}\Big|_{E=E_F} < 0$ at $V_G = -3.65\,V$. Thus, the characteristic of the carrier type of a certain molecular junction can be converted from n type (closer to LUMO) to p type (closer to HOMO) by tuning the gate voltage. In the unsubstituted butanethiol junction as shown in the right plane of Fig.8(b) [3], it is observed that the electron transmission function is always small because the location of the Fermi levels lies within the large HOMO-LUMO gap. We also note that the Seebeck coefficient has a negative value due to $\frac{\partial \ln\tau(E)}{\partial E}\Big|_{E=E_F} > 0$. When the gate voltages are further decreased, the absolute value of the Seebeck coefficient becomes bigger even in the unsubstituted butanethiol junction because the negative gate voltage shifts the LUMO peak toward the low-energy region.

The Seebeck coefficient is relevant to the temperatures of the electrodes. This property may be applied to the design of a molecular thermometer. To show this, we investigate the Seebeck coefficient of the amino-substituted butanrthiol junction at V_{SD}=0.01 V as a function of temperature of the left electrode (T_L) while keeping T_R=0 K as shown in Fig.8(c) [3]. The results show that the dependence of the Seebeck coefficient can be well described by Eq. (26), where T_R=0 K. As the temperature T_L becomes large, the approximation of Eq. (26) turns out to be inappropriate and the Seebeck coefficient shows nonlinear behavior. We further observe that the sensitivity of the Seebeck coefficient versus T_L can be amplified by applying gate voltages. At $V_G = -2.6\,V$, the Seebeck coefficient has a very small value insensitive to T_L because the peak of the transmission function lies between two Fermi levels. When the gate voltage is tuned to $V_G = -3.38\,V$, the Seebeck coefficient can be enhanced to around 38 μV/K at T_L=300 K. The other interesting phenomenon observed is the possibility to change the sign of the Seebeck coefficient by applying the gate voltage. When the gate voltage is tuned to $V_G = 1.72\,V$, the Seebeck coefficient becomes around −42 μV/K at T_L=300 K. The results show that the amino-substituted butanethiol may be an effective thermoelectric material applicable to the design of molecular thermoelectric devices such as thermometer.

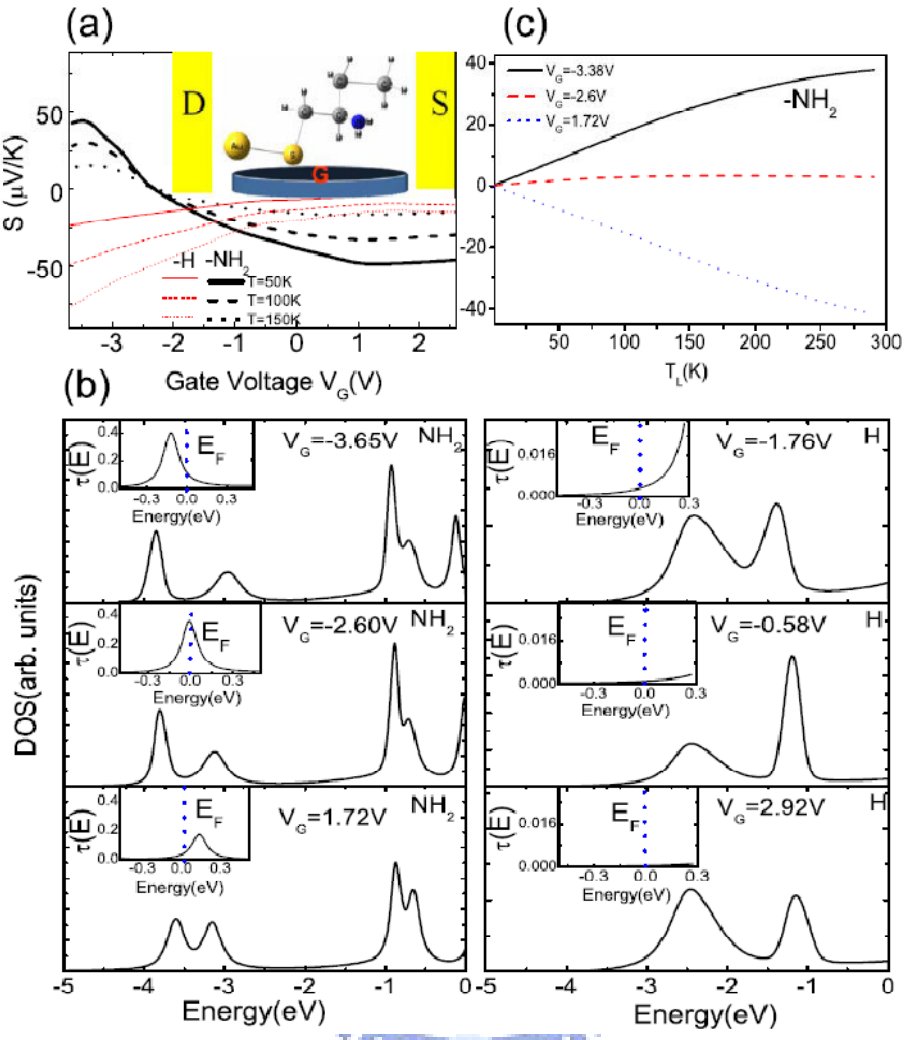

Fig. 8. The Seebeck coefficient S in a three-terminal geometry with V_{SD}=0.01 V: (a) S versus V_G where T_L=T_R=T for the amino-substituted [black (thick) lines] and unsubstituted [red (thin) lines] butanethiol for T=50 K (solid line), T=100 K (dashed line), and T=150 K (dotted line). The inset shows the schematic of the three-terminal junction. The gate field is applied in a direction perpendicular to the direction of charge transport. (b) The density of states and the transmission function (inset): the left panels for the amino-substituted butanethiol junction at V_G=-3.65, -2.60, and 1.72 V; the right panels are for the unsubstituted butanethiol junction at V_G=-1.76, -0.58, and 2.92 V. (c) S versus T_L for an amino-substituted butanethiol junction for V_G=-3.38, -2.60, and 1.72 V, where T_R=0 K. **[3]**

3-1-2 Seebeck coefficient in the nonlinear regime

The Seebeck coefficient of the amino-substituted (unsubstituted) butanethiol molecular junctions as a function of V_{SD} is plotted in Fig.9(b) [3](inset of Fig.9(b) [3]). At large V_{SD}, the difference between the left and right chemical potentials becomes significant. Thus, the transmission functions in the vicinity of both the left and right Fermi levels have important contribution to the Seebeck coefficient. In Fig.9(b) [3] we plot the DOSs and transmission functions as functions of the energy for various biases. For $V_{SD} > 0$, the states between the left and right Fermi levels are developed into a resonant peak similar to what is found in the elongated silicon point contact[24]. At large V_{SD}, the transmission functions around the left and right Fermi levels are equally important to the Seebeck coefficient [see Eq. (26)]. When T_L=T_R=T, we explain the Seebeck coefficient in Fig.9(a) [3] by considering the source-drain bias V_{SD} at 0.8, -0.3, and -0.5 V, respectively. For these biases, the contribution to the Seebeck coefficient is dominated by the transmission function in the vicinity of the left Fermi level. Thus, Eq. (26) can be further simplified as $S = -\frac{\pi^2 K_B^2 T}{3e}\frac{\partial \ln\tau(E)}{\partial E}\Big|_{E=\mu_L}$. The Seebeck coefficient is (negative; zero; positive) at $V_{SD} = (0.8; -0.3; -0.5)V$ because $\frac{\partial \ln\tau(E)}{\partial E}\Big|_{E=\mu_L}$ is $(>; \approx; < 0)$. We also observe that there are more zeroes in Seebeck coefficient as a function of V_{SD} in Fig.9(a) [3]. For example, at $V_{SD} = 0.2$ or -0.9 V, the peak position of the transmission function is located in the middle of the left and right Fermi levels such that $\frac{\partial \tau(E)}{\partial E}\Big|_{E=\mu_L} \approx -\frac{\partial \tau(E)}{\partial E}\Big|_{E=\mu_R}$. Consequently, the Seebeck coefficient is close to zero at $V_{SD} = 0.2$ and -0.9 V according to Eq. (26). In the unsubstituted butanethiol junction, the Seebeck coefficient as a function of V_{SD} is shown in the inset of Fig.9(a) [3]. The results show that the Seebeck coefficient remains a negative value in the whole bias regime owing to the fact that the Fermi levels are located between the large HOMO-LUMO gap.

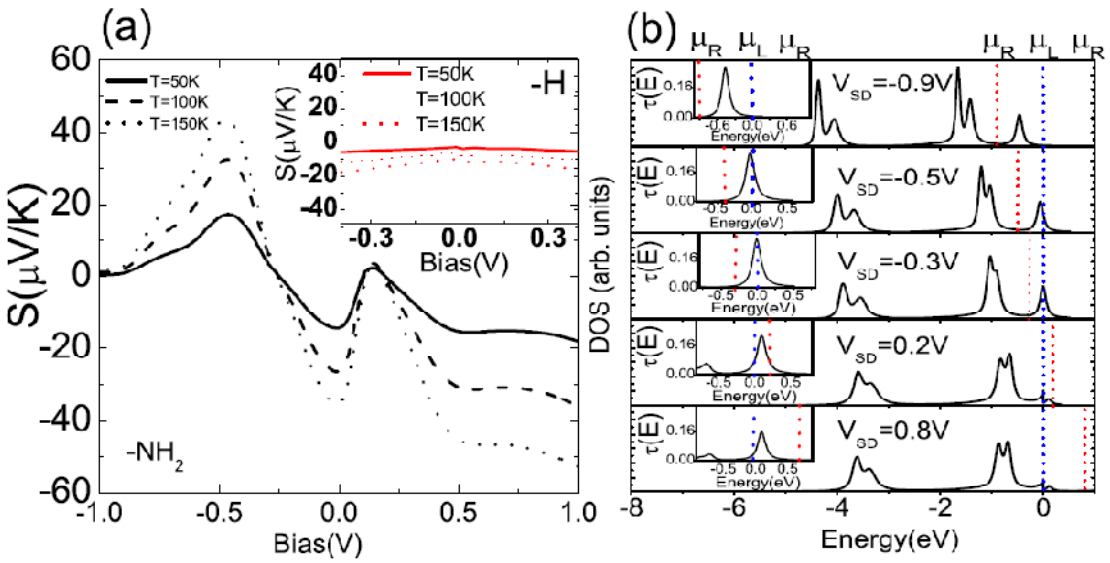

Fig. 9. (a) The Seebeck coefficient S as a function of source-drain biases in a two-terminal geometry for amino-substituted (main graph) and unsubstituted (inset in the upper right corner) butanethiol for T=50 K (solid lines), T=100 K (dashed lines), and T=150 K (dotted lines). (b) The density of states and the transmission function (inset) for various source-drain biases ($V_{SD} = -0.9$, -0.5, -0.3, 0.2, and 0.8 V) in the amino-substituted buanethiol junction. **[3]**

3-2 The comparison between Aluminum atomic junctions and Alkanethiol junctions[1,2]

In the followings, we investigate the thermoelectric figure of merit ZT in relation to the length characteristics of the junctions for metallic atomic wires and insulating molecular wires. We obtained the qualitative and quantitative descriptions for the dependence of ZT on temperatures and lengths.

3-2-1 Thermoelectric figure of merit

The properties of ZT now can be discussed using Eq. (34). There was a characteristic temperature, $T_0 \equiv \sqrt{\frac{\beta}{\gamma(\ell)}}$, for ZT in the nanojunctions. When $T \ll T_0$, the thermal current was dominated by the contribution from the electron transport ($\kappa_{ph} \ll \kappa_{el}$), which led to ZT increasing as the temperature increased: $ZT \approx \frac{\sigma S^2 T}{\kappa_{el}} \approx \left[\frac{\alpha^2\sigma}{\beta}\right] T^2$. Similarly, when $T \gg T_0$, the thermal current was dominated by the contribution from the phonon transport ($\kappa_{ph} \gg \kappa_{el}$), which led to a saturation of ZT at a constant value related to the length of the junction: $ZT \approx \frac{\sigma S^2 T}{\kappa_{ph}} \approx \frac{\alpha^2\sigma}{\gamma(\ell)}$. To increase ZT it was first necessary to reduce κ_{ph} by choosing low-elasticity bridging wires or creating poor thermal contacts in the nanojunctions, such that $ZT \approx \frac{\sigma S^2 T}{\kappa_{el}}$. It is worth noting that σ and κ_{el} roughly canceled each other out in the contribution of ZT because both were proportional to $\tau(\mu)$. It then followed that $ZT \propto S^2$ and, thus, that the material with a large Seebeck coefficient was of key importance to increasing ZT. In addition, it was noted that α and σ depend on the length of the junction in a way related to the material properties of bridging wires, which is reflected in the distinguished features of ZT on the length dependence. This point was explained using two

catalogs of nanojunctions: the aluminum atomic (conducting) wires and the alkanethiol (insulating).

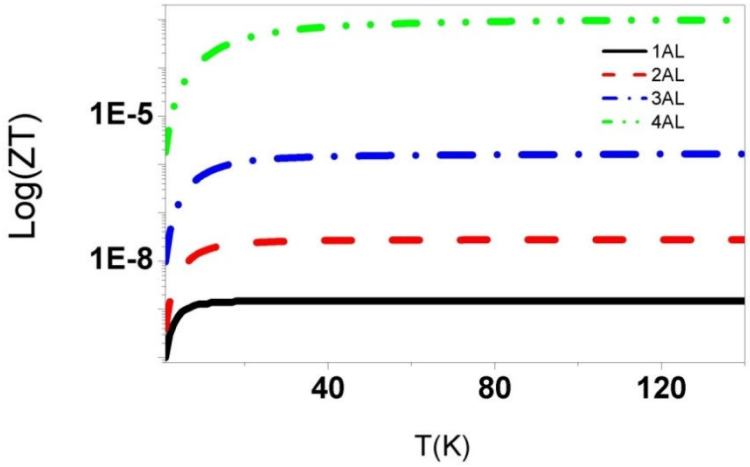

Fig. 10. Aluminum atomic junctions at $V_B = 0.01\,V$ and $T_L \approx T_R = T$: Log(ZT) versus T ($Y \simeq 1.2 \times 10^{13}$ dyne/cm^2). **[1]**

Fig.10 [1] shows ZT with κ_{ph} calaulated using $Y = 1.2 \times 10^{13}$ dyne/cm^2 from the total energy calculations. The increase in the number of Al atoms sharply increased the saturation value of ZT because of the sharp increase in Seebeck coefficient by the number of Al atoms according to $ZT \propto S^2$. ZT reached the saturation value, $ZT \rightarrow \frac{\alpha^2\sigma}{\gamma(\ell)}$ when $T \gg T_0$.

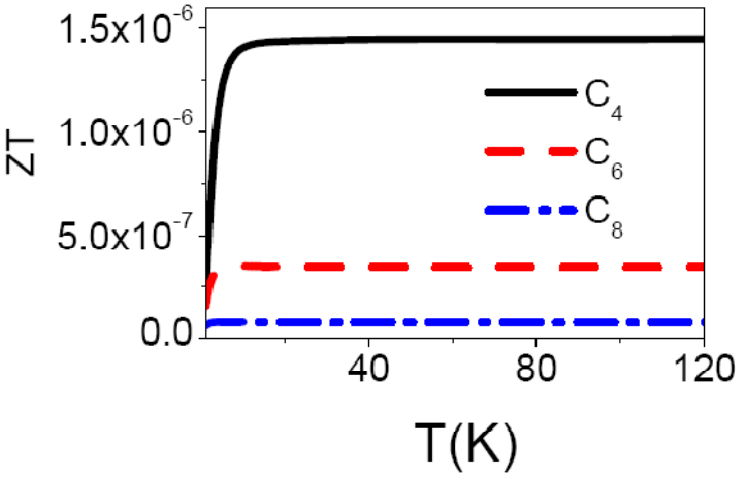

Fig. 11. Alkanethiol junctions at $V_B = 0.01\,V$ and $T_R \approx T_L \approx T$: ZT versus T ($Y \simeq 2.3 \times 10^{12}$ dyne/cm^2). **[1]**

Due to the small transmission probability for the insulating alkanethiol chains, the electron thermal conductance (note: $\kappa_{el} \propto \sigma$) was much suppressed so that $\kappa_{el} \ll \kappa_{ph}$, as shown in Fig.17 [1] and Fig.19 [1]. Consequently, the characteristic temperature T_0 was low in the alkanethiol chains, and the T^2 regime for ZT was significantly suppressed. As shown in Fig.11 [1], ZT decreased as the number of carbon atoms increased for $T \gg T_0$, due to the saturation value of $ZT \approx \frac{\alpha^2\sigma}{\gamma(\ell)} \propto \ell^2 e^{-\xi\ell}$.

3-2-2 Seebeck coefficient

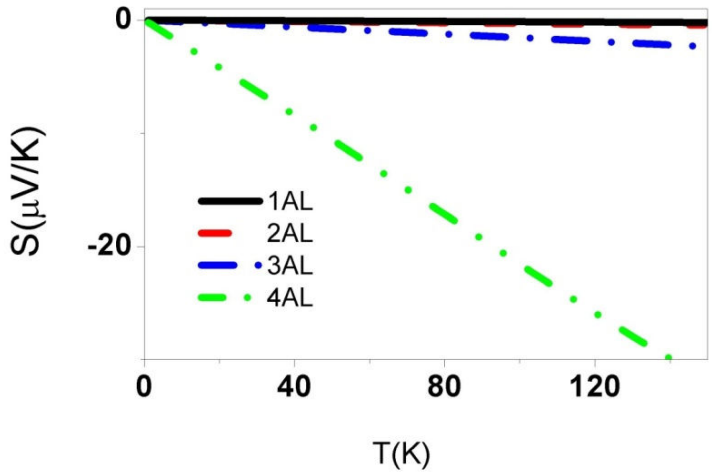

Fig. 12. Aluminum atomic junctions at $V_B = 0.01\,V$ and $T_L \approx T_R = T$: Seebeck coefficients S versus T. **[1]**

As shown in Fig.12 [1], the magnitude of the Seebeck coefficient was linear in temperature, $S \approx \alpha T$, with the negative sign showing that the carrier was n-type. At a fixed temperature, it was observed that the magnitude of the Seebeck coefficient increased considerably as the number of Al atoms increased. The increase of the Seebeck coefficient was due to the increase of the slope in the DOS at the Fermi level. These features may be related to the fact that the Fermi level was close to the LUMO in the Al wires.

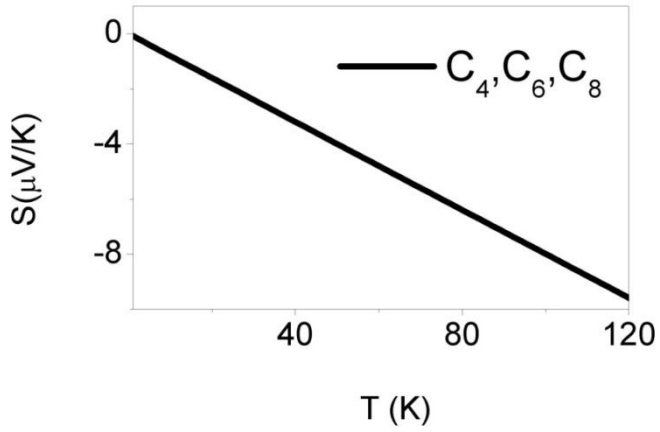

Fig. 13. Alkanethiol junctions at $V_B = 0.01\,V$ and $T_R \approx T_L \approx T$: Seebeck coefficients S versus T. **[1]**

As shown in Fig.13 [1], the magnitude of the Seebeck coefficient was linear in temperature as $S \approx -\frac{\pi^2 K_B^2}{3e\tau(\mu)}\frac{\partial\tau(\mu)}{\partial E}T$, and its dependence on the number of carbon atoms was canceled due to the same scaling factor $e^{-\xi\ell}$ for both $\tau(\mu)$ and $\frac{\partial\tau(\mu)}{\partial E}$.

3-2-3 Electrical conductance

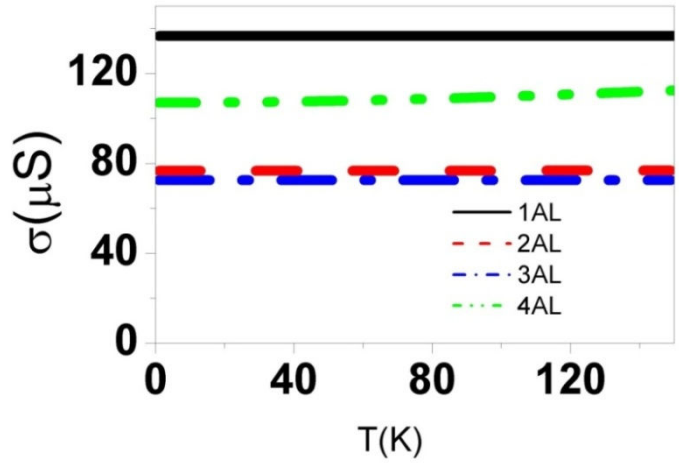

Fig. 14. Aluminum atomic junctions at $V_B = 0.01\,V$ and $T_L \approx T_R = T$: Electric conductance σ versus T. **[1]**

As shown in Fig.14 [1], the conductance was relatively insensitive to the

chain length (typically around $1G_0 = \frac{2e^2}{h} \approx 77\mu S$) apart from the possible 4-atom periodicity due to a filling factor of $\frac{1}{4}$ in the π orbitals[25].

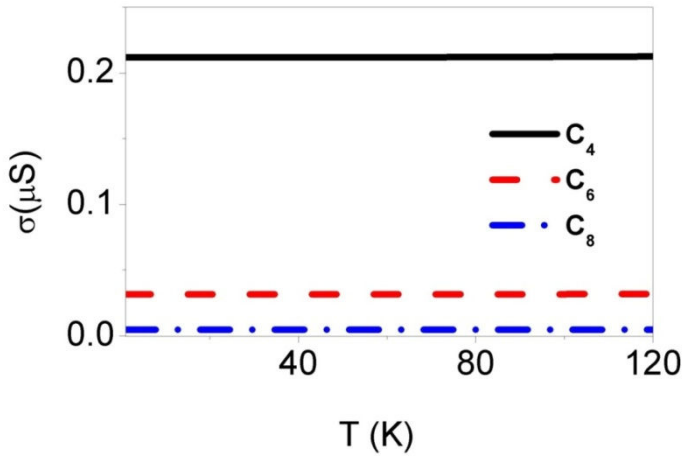

Fig. 15. Alkanethiol junctions at $V_B = 0.01\,V$ and $T_R \approx T_L \approx T$: Electric conductance σ versus T. **[1]**

In contrast to the conductor behavior of aluminum wires, alkanethiol chains are insulators. It has been established that non-resonant tunneling is the main conduction mechanism in alkanethiol junctions. Consequently, the conductance is small and decreases exponentially with the length of wire, as $\sigma = \sigma_0 e^{-\xi \ell}$ where ℓ is the length of alkanethiol chain and $\xi \approx 0.78 Å^{-1}$[26,27,28,29,30], as shown in Fig.15 [1]. By exploiting the periodicity in the $(CH_2)_2$ group of the alkanethiol chains, the wave functions of the C_n junctions were calculated by a scaling argument, which led to exponential scaling in the transmission function $\tau(\mu)$.

3-2-4 Electron thermal conductance

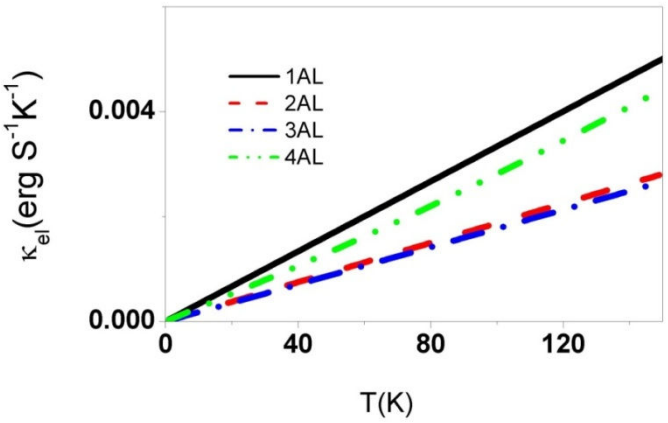

Fig. 16. Aluminum atomic junctions at $V_B = 0.01\,V$ and $T_L \approx T_R = T$: Electron thermal conductance κ_{el} versus T. **[1]**

As shown in Fig.16 [1], the magnitude of electron thermal conductance was linear in temperatures, $\kappa_{el} \approx \beta T$. At a fixed temperature, the dependence of the magnitude of κ_{el} on the number of Al atoms was the same as that of σ, owing to the fact that both σ and κ_{el} were proportional to $\tau(\mu)$.

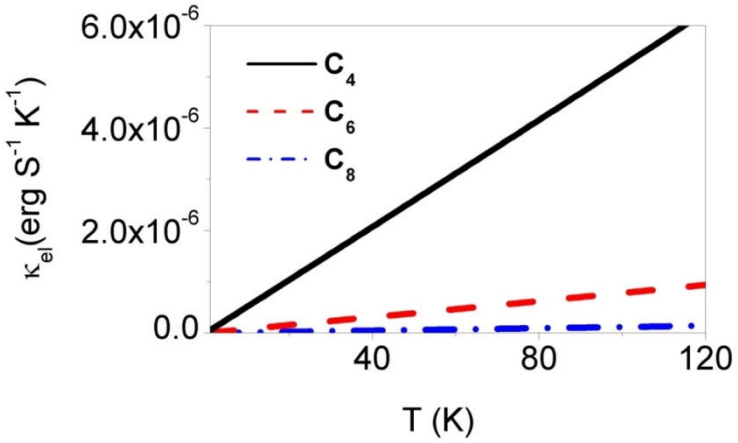

Fig. 17. Alkanethiol junctions at $V_B = 0.01\,V$ and $T_R \approx T_L \approx T$: Electron thermal conductance κ_{el} versus T. **[1]**

As shown in Fig.17 [1], the magnitude of electron thermal conductance was linear in temperatures, $\kappa_{el} \approx \beta T$. At a fixed temperature, the magnitude of κ_{el} decreased exponentially with n, the number of carbon atoms in C_n , owing to the scaling behavior of $\tau(\mu)$.

3-2-5 Phonon thermal conductance

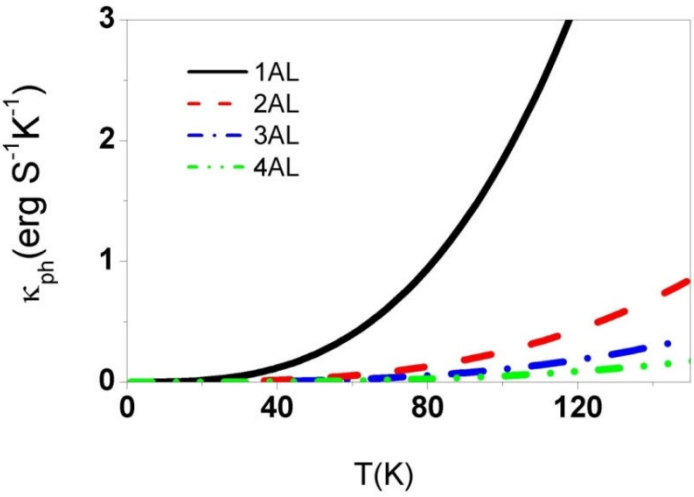

Fig. 18. Aluminum atomic junctions at $V_B = 0.01\,V$ and $T_L \approx T_R = T$: Phonon thermal conductance κ_{ph} versus T ($Y \simeq 1.2 \times 10^{13}$ dyne/cm^2). **[1]**

Fig.18 [1] shows the phonon thermal conductance: $\kappa_{ph} = \gamma(\ell)T^3$, for the Young modulus using $Y = 1.2 \times 10^{13}$ dyne/cm^2 from the total energy calculations. As seen, $\kappa_{ph} \gg \kappa_{el}$ was due to the large Young modulus.

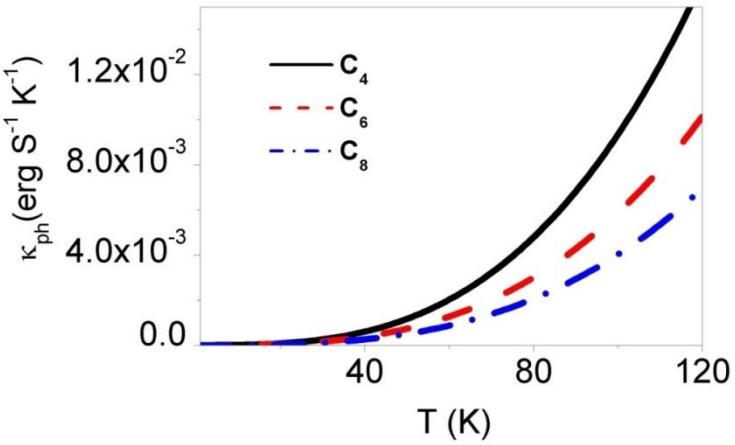

Fig. 19. Alkanethiol junctions at $V_B = 0.01\,V$ and $T_R \approx T_L \approx T$: Phonon thermal conductance κ_{ph} versus T ($Y \simeq 2.3 \times 10^{12}$ dyne/cm^2). **[1]**

As shown in Fig.19 [1], thermal conductance increased as the temperature increased as $\kappa_{ph} = \gamma(\ell)T^3$ for the Young modulus calculated with total energy calculations. At a fixed temperature, κ_{ph} decreased as n^{-2} due to $\gamma(\ell) \propto \ell^{-2}$.

The relation between ZT and the wire lengths depended on the material properties: for aluminum atomic (conducting) wires, the saturation value of ZT increased as the length increased; while for the alkanethiol (insulating) chains, the saturation value of ZT decreased as the length increased.

The insulating molecular junctions reveal partial material properties, where the thermoelectric physical quantities are irrelevant to the sizes and shapes of materials. For example, the Seebeck coefficient is insensitive to the length of junction and show material properties. The thermoelectric figure of merit possess partial material properties since ZT depends on the lengths of nanojunctions: $ZT \propto \ell^2 e^{-\xi\ell}$, while the dependence of ZT on length characteristic in nanojunctions could be frustrated in case that the phonon thermal conductance is absent. i.e., $\kappa_{ph} = 0$. In any case, the metallic atomic junctions show strong junction properties, which could be in credited to the strong hybridization between the electronic structure of metallic chains and the electrodes. We believe it is a substantial step forward to illustrate that thermoelectric nanojunctions maintain junction properties and hope that our results will generate more experimental and theoretical explorations on the junction properties of the thermoelectric nanojunctions.

Chapter 4 Conclusion

First, we have investigated the thermoelectricity in the molecular junctions in both linear and nonlinear regimes. The Seebeck coefficients are studied using first-principles calculations. The general properties of the Seebeck coefficient effects can be very different for the unsubstituted and amino-substituted butanethiol junctions in the two-terminal and three-terminal molecular geometries. The research illustrates that the gate field is able to modulate and optimize the Seebeck coefficient. Another interesting phenomenon is the possibility to change the signs of the Seebeck coefficient by applying the gate voltages and biases in amino-substituted butanethiol junction. It is observed that the Seebeck coefficient is relevant to the temperatures of the electrodes that may be applied to the design of a molecular thermometer and its sensibility can be controlled by gate voltages. We also extend the investigation of the Seebeck coefficient to molecular tunnel junction at finite biases. As the biases increase, richer features in the Seebeck coefficient are observed, which are closely related to the transmission functions in the vicinity of the left and right Fermi levels. All results show that the molecular tunnel junction based on alkanethiols may be a promising candidate for the design of novel thermoelectric devices in the future.

Second, we have investigated (metallic) aluminum atomic junctions and (insulating) molecular junctions at very low source-drain bias (in the linear response regime), and temperature T_R, T_L ($T_R \approx T_L \approx T$) in both electrode. We can get some conclusion as below:

For $T \ll T_0$, $ZT \to (\frac{\alpha^2\sigma}{\beta})T^2$; for $T \gg T_0$, ZT trend to a saturation value, $\frac{\alpha^2\sigma}{\gamma(\ell)}$.

And the key importance to increase ZT is using material with large Seebeck coefficient. Such materials are characterized by a sharp peak around the Fermi levels.

The relation between ZT and the wire lengths depended on the material properties: for aluminum atomic (conducting) wires, the saturation value of ZT increased as the length increased; while for the alkanethiol (insulating) chains,

the saturation value of ZT decreased as the length increased.

We show that the thermoelectric quantities in nanojunctions unnecessarily display material properties. The Seebeck coefficient and the thermoelectric figure of merit are shows that metallic atomic chains reveal strong junction properties while the insulating molecular wires partially possess the material properties.

Reference

1. Y. S. Liu, Y. R. Chen and Y. C. Chen, “Efficiency of Energy Conversion in Thermoelectric Nanojunctions”, cond-mat/arXiv:0902.3876 (2009).
2. Y. C. Chen and Y. S. Liu , “Thermoelectric Materials in Nanojunctions Display Material Property or Junction Property?”, cond-mat/arXiv:0904.0692 (2009).
3. Y. S. Liu and Y. C. Chen, “Seebeck coefficient of thermoelectric molecular junctions: First-principles calculations”, Phys. Rev. B 79, 193101 (2009).
4. E. Altenkirch, Phys. Zeitschrift 10 (1909) 560-580.
5. E. Altenkirch, Phys. Zeitschrift 12 (1911) 920-924.
6. A. F. Ioffe, “Semiconductor Thermoelements and Thermoelectric Cooling”, Infosearch, London, 1957.
7. T.Markussen, A. P. Jauho and M.Brandbyge, “Electron and phonon transport in silicon nanowires: Atomistic approach to thermoelectric properties”, Phys. Rev. B 79, 035415 (2009).
8. X. Zheng, W. Zheng, Y. Wei, Z. Zeng and J. Wang, J. Chem. “Thermoelectric transport properties in atomic scale conductors”, Phys. 121, 8537 (2004).
9. T. J. Seebeck, Proc. Prussian Acad. Sci. (1822) 265-373.
10. J. C. Peltier, Ann. Chem.LVI (1834) 371-387.
11. W. Thomson, Proc. Roy. Soc. Edinburgh (1851) 91-98.
12. P. Reddy, S. Y. Jang, R. A. Segalman and A. Majumdar, “Thermoelectricity in Molecular Junctions”, Science 315, 1568 (2007).
13. K. Baheti, J. A. Malen, P. Doak, P. Reddy, S. Y. Jang, T. D. Tilley, A. Majumdar and R. A. Segalman, “Probing the Chemistry of Molecular Heterojunctions Using Thermoelectricity”, Nano Lett. 8, 715 (2008).
14. J. A. Malen, P. Doak, K. Baheti, T. D. Tilley, R. A. Segalman and A. Majumdar, “Identifying the Length Dependence of Orbital Alignment and Contact Coupling in Molecular Heterojunctions”, Nano Lett. 9, 1164 (2009).

15. M. Büttiker, Y. Imry, R. Landauer, S. Pinhas, “Generalized many-channel conductance formula with application to small rings”, Phys. Rev. B 31, 6207 (1985).
16. N. D. Lang, “Resistance of atomic wires”, Phys. Rev. B 52, 5335 (1995).
17. G. B. Bachelet, D. R. Hamann and M. Schlüter, “Pseudopotentials that work: From H to Pu”, Phys. Rev. B 26, 4199 (1982).
18. M. Di Ventra, S.T. Pantelides and N. D. Lang, “The benzene molecule as a molecular resonant-tunneling transistor”, Appl. Phys. Lett. 76, 3448 (2000).
19. Z. Yang, A. Tackett and M. Di Ventra, “Variational and nonvariational principles in quantum transport calculations”, Phys. Rev. B 66, 041405 (2002).
20. B. Wang, Y. Xing, L. Wan, Y. Wei and J. Wang, “Oscillatory thermopower of carbon chains: First-principles calculations”, Phys. Rev. B 71, 233406 (2005).
21. K. R. Patton and M. R. Geller, “Thermal transport through a mesoscopic weak link”, Phys. Rev. B 64, 155320 (2001).
22. W. Wang, T. Lee and M. A. Reed, “Mechanism of electron conduction in self-assembled alkanethiol monolayer devices”, Phys. Rev. B 68, 035416 (2003).
23. N. J. Tao, “Electron transport in molecular junctions”, Nat. Nanotechnol., 1, 173 (2006).
24. M. Di Ventra, Y. C. Chen, and T. N. Todorov, “Are Current-Induced Forces Conservative?”, Phys. Rev. Lett. 92, 176803 (2004).
25. K. S. Thygesen and K. W. Jacobsen, “Four-Atom Period in the Conductance of Monatomic Al wires”, Phys. Rev. Lett. 91, 146801 (2003).
26. D. J. Wold and C. D. Frisbie, “Fabrication and Characterization of Metal-Molecule-Metal Junctions by Conducting Probe Atomic Force Microscopy”, J. Am. Chem. Soc., 123, 5549 (2001).
27. J. M. Beebe, V. B. Engelkes, L. L. Miller and C. D. Frisbie, “Contact Resistance in Metal-Molecule-Metal Junctions Based on Aliphatic SAMs: Effects of Surface Linker and Metal Work Function”, J. Am. Chem. Soc.,

124,11268 (2002).

28. J. Zhao and K. Uosaki, “Formation of Nanopatterns of a Self-Assembled Monolayer (SAM) within a SAM of Different Molecules Using a Current Sensing Atomic Force Microscope”, Nano Lett., 2, 137 (2002).
29. C. C. Kaun and H. Guo, “Resistance of Alkanethiol Molecular Wires”, Nano Lett., 3, 1521 (2003).
30. C. L. Ma, D. Nghiem and Y. C. Chen, “Alkanethiol-based single-molecule transistors”, Appl. Phys. Lett., 93,222111 (2008).